JACS
JOURNAL OF THE AMERICAN CHEMICAL SOCIETY

ARTICLE

pubs.acs.org/JACS

Proton-Coupled Electron-Transfer Processes in Photosystem II Probed by Highly Resolved *g*-Anisotropy of Redox-Active Tyrosine Y_Z

Hideto Matsuoka,*[,†] Jian-Ren Shen,[‡] Asako Kawamori,[§] Kei Nishiyama,[†] Yasunori Ohba,[†] and Seigo Yamauchi[†]

[†]Institute of Multidisciplinary Research for Advanced Materials, Tohoku University, Katahira-2-1-1, Aobaku, Sendai 980-8577, Japan

[‡]Graduate School of Natural Science and Technology, Department of Biology, Faculty of Science, Okayama University, Naka-Tsushima, Okayama 700-8530, Japan

[§]Agape-Kabutoyama Institute of Medicine, Kabutoyama-cho 54-3, Nishinomiya 662-0001, Japan

Supporting Information

ABSTRACT: The oxidation of a redox-active tyrosine residue Y_Z in photosystem II (PSII) is coupled with proton transfer to a hydrogen-bonded D1-His190 residue. Because of the apparent proximity of Y_Z to the water-oxidizing complex and its redox activity, it is believed that Y_Z plays a significant role in water oxidation in PSII. We investigated the *g*-anisotropy of the tyrosine radical $Y_Z^{\bullet}$ to provide insight into the mechanism of $Y_Z^{\bullet}$ proton-coupled electron transfer in Mn-depleted PSII. The anisotropy was highly resolved by electron paramagnetic resonance spectroscopy at the W-band (94.9 GHz) using PSII single crystals. The g_X-component along the phenolic C−O bond of $Y_Z^{\bullet}$ was calculated by density functional theory (DFT). It was concluded from the highly resolved *g*-anisotropy that Y_Z loses a phenol proton to D1-His190 upon tyrosine oxidation, and D1-His190 redonates the same proton back to $Y_Z^{\bullet}$ upon reduction.

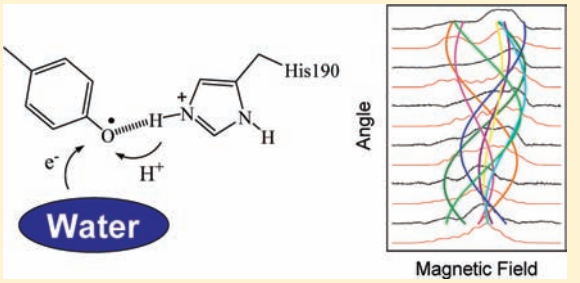

INTRODUCTION

Photosystem II (PSII) catalyzes water oxidation in plants and cyanobacteria using solar energy, leading to the formation of molecular oxygen. Within PSII, molecular oxygen is produced from water by the water-oxidizing complex (WOC), which is composed of four exchange-coupled manganese (Mn) atoms and one calcium (Ca) atom. The crystal structure of PSII in two species of cyanobacterium, *Thermosynechococcus elongatus* and *Thermosynechococcus vulcanus*, has recently been reported.[1−3] The unit cell contains four sites related by the $P2_12_12_1$ space group, each of which is composed of a dimer of the PSII core complex. The individual core complexes are related to each other by a noncrystallographic C_2 symmetry axis parallel to the membrane normal. Each PSII monomer contains two redox-active tyrosine residues, Tyr 161 (Y_Z) in the D1 polypeptide and Tyr 160 (Y_D) in the D2 polypeptide. High-frequency electron paramagnetic resonance (EPR) studies have provided detailed information on the electronic and molecular structures of redox-active molecules in PSII.[4−6] The *g*-tensors and their orientation relative to the crystal axes have been precisely determined for the tyrosine radical $Y_D^{\bullet}$[5,6] and WOC[7] by W-band (94 GHz) EPR studies on single crystals of PSII.

A number of accounts have addressed mechanistic details of the oxidization of water by WOC.[8−10] It has been suggested that Y_Z plays a significant role in water oxidation. Y_Z serves as an intermediate in electron transfer from WOC to the primary chlorophyll donor P_{680}. Oxidation of Y_Z by P_{680}^{+} leads to the formation of a neutral radical, $Y_Z^{\bullet}$.[11] Because the reduced form of Y_Z is expected to be protonated, a proton must be transferred between Y_Z and a nearby base during Y_Z oxidation (Figure 1). On the basis of a number of site-directed mutagenesis studies, it was suggested that the proton acceptor in oxidized Y_Z is D1-His190.[12] This was confirmed by a recent crystal structure analysis showing that Y_Z is within H-bonding distance of D1-His190. Babcock and co-workers proposed that Y_Z participates directly in water oxidation by abstracting hydrogen atoms from water bound to WOC (H-abstraction mechanism), as shown in Figure 2a.[13] In contrast to this H-abstraction hypothesis, Renger and co-workers suggested that one proton remains near Y_Z (Figure 2b), moving only the small distance between Y_Z and D1-His190, depending on the redox state of Y_Z (proton-rocking mechanism).[14−16] To determine the function of Y_Z in the catalytic water oxidation process, it is important to determine the *g*-anisotropy of Y_Z, which is very sensitive to the electrostatic environment.[4] In this study, the *g*-anisotropy of the tyrosine radical $Y_Z^{\bullet}$ in Mn-depleted PSII was highly resolved by W-band (94.9 GHz) EPR spectroscopy to discriminate between the two possible mechanisms. This is the first EPR measurement of $Y_Z^{\bullet}$ in PSII single crystals. Combined with density functional theory (DFT) theoretical calculations, the highly resolved *g*-anisotropy allowed us to probe the PCET (proton-coupled electron-ransfer) processes accompanying

Received: January 15, 2011
Published: March 07, 2011

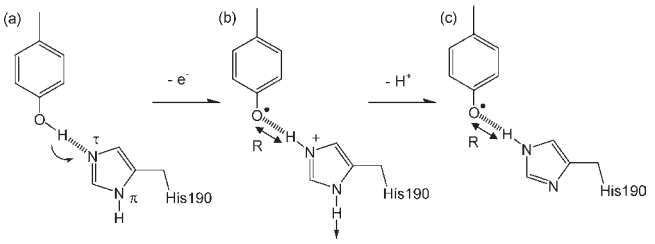

Figure 1. Schematic representation of photooxidation of the redox-active tyrosine molecule Y_Z: (a) reduced form, (b) tyr−imidazolium ion complex, and (c) tyr−imidazole complex.

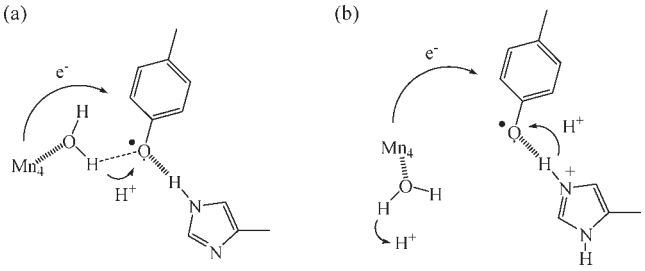

Figure 2. Proposed mechanisms for water oxidation: (a) H-atom abstraction,[13] and (b) proton-rocking[14−16] pathways.

tyrosine oxidation. In addition, the molecular orientations of $Y_Z^\bullet$ in single crystals of PSII were determined precisely through the principal axis orientation of the *g*-tensor.

EXPERIMENTAL METHODS

Sample Preparation. Cells of the thermophilic cyanobacterium *T. vulcanus* were grown, and core particles of PSII were isolated as described previously.[17] To remove Mn from WOC, PSII samples were treated with 2 mM NH_2OH in a buffer containing 20 mM Mes (pH 6.0), 10 mM NaCl, and 3 mM $CaCl_2$ at a chlorophyll concentration of 0.5 mg/mL for 30 min on ice in the dark, and then precipitated by centrifugation and resuspended in the same buffer. This treatment was repeated, and finally the samples were suspended in the same buffer without NH_2OH but supplemented with 0.5 mM potassium ferricyanide and 30% glycerol.

Single crystals of PSII were grown as described previously.[17] Well-defined crystals with an approximate size of 0.4 × 0.2 × 0.6 mm^3 were used for measurements. The crystals were harvested in the mother liquor supplemented with 2 mM NH_2OH, and then dialyzed against a cryo-protectant solution containing 25% glycerol, 20% polyethylene glycol 1450, and 2 mM NH_2OH for 4 h at 20 °C. Following dialysis, the crystals were transferred into a fresh cryo-protectant solution without NH_2OH but supplemented with 0.5 mM potassium ferricyanide, and then inserted into quartz capillaries with an outer diameter of 0.9 mm. The remaining solution in the capillary tubes was quickly removed, and the crystals were then frozen with liquid nitrogen.

EPR Spectroscopy. A pulsed W-band spectrometer was constructed by incorporating a pulsed microwave bridge and a laboratory-made PC control system into a Bruker E600 spectrometer. The bridge is the so-called "Krymov bridge" that has now been installed in several laboratories.[18,19] The apparatus operated at 94.9 GHz. The sample temperature inside the EPR cavity was controlled by a helium flow cryostat (Oxford Instruments ,odel CF935) and a temperature controller (Oxford Instruments model ITC500). To generate the neutral radical $Y_Z^\bullet$, the NH_2OH-treated solution and crystal samples were illuminated for 20 s at 253 K in the cavity with continuous light from a 150 W xenon lamp guided by an optical fiber. The samples were cooled rapidly under illumination to trap the radicals, and the light was turned off at 200 K. The temperature was then further decreased to 80 K, where W-band measurements were performed. For measurement of dark-annealed spectra, the temperature of the samples in the cavity was increased to 253 K, and annealing was allowed to take place for 30 min in the dark. Orientation-dependent spectra of $Y_D^\bullet$ and $Y_Z^\bullet$ were recorded by repeatedly rotating single-crystal samples by 15° about the capillary axis perpendicular to the magnetic field. EPR measurements in two planes of rotation were obtained by using two single crystals with different orientations relative to the capillary axis. Field-swept electron spin echo (ESE) signals were obtained using a two-pulse ($\pi/2-\tau-\pi$) microwave sequence; the values of $\pi/2$ and τ were 50 and 250 ns, respectively.

EPR Spectral Simulation. The *g*-values and hyperfine coupling constants of the tyrosine radicals were determined by computer simulation. One of the authors had in previous work determined the hyperfine coupling constants of $Y_D^\bullet$ and $Y_Z^\bullet$ by X-band pulsed electron nuclear double resonance spectroscopy.[20] In this work, the coupling constants were refined through computer simulation of W-band EPR from single crystals of PSII (see the Supporting Information). Computer simulation of EPR spectra was carried out by a modified program based on second-order perturbation theory,[6,21] which was constructed using the MATLAB 6.5 program from The MathWorks, Inc. In this program, resonance fields and transition intensities were calculated using analytical expressions derived by Iwasaki.[22]

DFT Calculations. For geometric optimization of $Y_Z^\bullet$ and *g*-tensor calculation, the B3LYP hybrid DFT method, as implemented in the Gaussian 03 package, was used. The geometries of the isolated $Y_Z^\bullet$ radical and the tyrosine−histidine complexes were optimized at the B3LYP/6-31++G** level. The EPR-III and 6-311++G** basis sets were used to calculate the magnetic properties of the radical species at the optimized geometries. The *g*-tensor was calculated by the gauge-independent atomic orbital method, as implemented in Gaussian 03. The dependence of the *g*-tensor upon basis set and density functional has also been examined (see the Supporting Information). The effect of the protein environment on the *g*-tensor was also investigated by COSMO (conductor-like screening model),[23] as implemented in the Orca 2.8.01 (Frank Neese, University of Bonn) using coupled-perturbed DFT theory.[24] Assuming that the dielectric constant is 2,[25] geometry optimizations and the *g*-tensor calculations were performed at the B3LYP/TZVP level and the B3LYP/EPR-II level, respectively.

RESULTS AND DISCUSSION

DFT Theoretical Investigations of the g_x-Component for $Y_Z^\bullet$. The *g*-tensor of organic π radicals deviates from the free-electron *g*-value (2.0023) depending on the spin density in the out-of-plane 2p orbital of heteroatoms possessing in-plane lone pairs. A pronounced deviation can be seen when the heteroatoms are involved in hydrogen bonding.[4] Here, the hydrogen-bonding environment of a radical was investigated through the *g*-tensor with the help of DFT calculations.[26,27] Figure 3 shows the orientation of the *g*-tensor with respect to the molecular frame of the tyrosine radical: g_x is directed along the phenolic C−O bond, g_z is perpendicular to the phenyl ring plane, and g_y is mutually perpendicular to the other two components.[28] DFT calculations were performed to investigate whether the *g*-anisotropy of $Y_Z^\bullet$ could clarify the PCET mechanism during photooxidation of the redox-active tyrosine Y_Z. On the basis of X-ray crystallographic analysis[1] and site-directed mutagenesis,[12] it is very likely that the phenolic hydrogen of the redox-active tyrosine molecule Y_Z is involved in hydrogen-bond donation to the τ-nitrogen of the imidazole group of D1-His190

dx.doi.org/10.1021/ja2000566 |J. Am. Chem. Soc. 2011, 133, 4655–4660

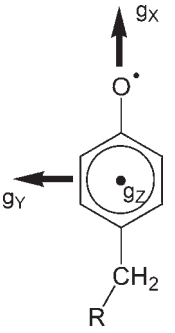

Figure 3. Orientation of the *g*-tensor in tyrosyl radicals as determined by Fasanella and Gordy.[28]

(Figure 1a), resulting in the formation of an imidazolium ion in D1-His190 (tyr—imidazolium ion complex) after photooxidation (Figure 1b). Deprotonation of the π-nitrogen of the imidazole group leads to a neutral tyrosyl—imidazole complex, as shown in Figure 1c.

Initially, the tyr—imidazolium ion complex and the tyr—imidazole complex were optimized geometrically, and then variations in the *g*-values accompanying changes in the hydrogen-bond length were calculated by the gauge-independent atomic orbital method in Gaussian 03. The hydrogen-bond lengths in the optimized structures of the reduced tyrosine—histidine complex, the tyr—imidazole complex, and the tyr—imidazolium ion complex are 1.83, 1.92, and 1.60 Å, respectively (*R* in Figure 1). The two planes containing the phenoxy and imidazole rings are almost orthogonal in the neutral complexes (Figure 1a and c) but are coplanar in the cationic complex (Figure 1b). The *g*-tensor of the tyrosine radical was not affected by the mutual orientation of the histidine molecule and the radical, as shown in the literature.[29] Figure 4a and b shows the dependence of the calculated g_x-value on the hydrogen-bond length. It was demonstrated from the DFT calculations that the *g*-tensor orientations with respect to the molecular frame in the hydrogen-bonded forms are almost coincident with those of the isolated neutral radical. It can be clearly seen that the g_x-value increases with increasing hydrogen-bond length, but the g_y and g_z-values are essentially unaffected by the hydrogen-bond length (not shown here). The *g*-tensor calculation at the optimized geometry (R = 1.60 Å) for the tyr—imidazolium ion complex produced a g_x-value of 2.0072. However, even for the shortest hydrogen-bond length of 1.5 Å (strong hydrogen bonding, Figure 4a), a g_x-value of 2.0089 was obtained for the tyr—imidazole complex.

The effect of the protein environment on the g_x-component was investigated using the COSMO with the dielectric constant of 2.[25] The hydrogen-bond lengths in the optimized structures of the tyr—imidazole and the tyr—imidazolium ion complexes are 1.92 and 1.66 Å, respectively. The *g*-tensor calculations at the optimized geometries produced the g_x-values of 2.0084 and 2.0068 for the tyr—imidazole and the tyr—imidazolium ion complexes, respectively. It was demonstrated that the protein environment has little effect on the *g*-tensor. It is worth noting that the *g*-tensors of phenoxyl radicals hydrogen-bonded to an imidazolium group were reproduced in an organic solvent with sufficient accuracy (100 ppm) using COSMO at the B3LYP/EPR-II level.[29]

Babcock and co-workers proposed the intervention of a H-atom abstraction pathway in water oxidation,[13] as shown in

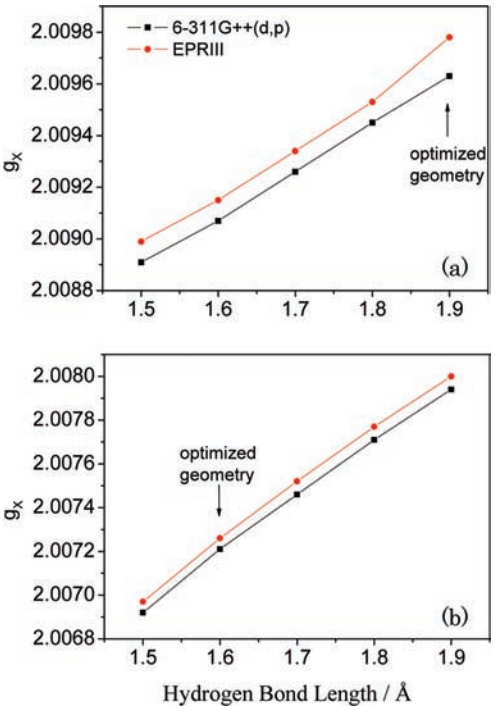

Figure 4. Dependence of the g_X-value on hydrogen-bond length, calculated for (a) the tyr—imidazole complex and (b) the tyr—imidazolium ion complex. The hydrogen-bond length *R* is defined in Figure 1.

Figure 2a. In this mechanism, deprotonation from the imidazolium ion, that is, the formation of a tyr—imidazole complex, is required because hydrogen atoms from water molecules must be delivered to the protein surface via D1-His190. However, in the proton-rocking mechanism proposed by Renger and co-workers, the proton in the imidazole group is "rocked" on the imidazole ring and transferred back to Y_Z upon rereduction by WOC (Figure 2b),[14−16] which does not require the formation of a tyr—imidazole complex. DFT investigations of *g*-anisotropy allow discrimination between the tyr—imidazolium ion and the tyr—imidazole complexes.

Resolution of the *g*-Anisotropy of $Y_Z^\bullet$. Orientation-dependent W-band EPR spectra of $Y_Z^\bullet$ were obtained by repeatedly rotating a single crystal of Mn-depleted PSII by 15°. EPR measurements in two planes of rotation were achieved by using two single crystals with different orientations relative to the capillary axis of the sample. The experimental spectra, which correspond to the light minus dark-annealed difference spectra, are depicted in Figure 5b as black lines at 30° intervals. To ensure that the light minus dark-annealed difference spectra were correct, a color center of quartz capillary tubes was employed as an internal intensity standard with EPR signals at around 3.3888 T (shown by an asterisk in Figure 6a). The *g*-anisotropy of $Y_Z^\bullet$ was determined by computer simulation. The space group of PSII crystals is $P2_12_12_1$,[1−3] with one unit cell composed of four PSII complexes. Because the PSII complex is a dimer in its crystalline form, each unit cell includes eight PSII monomers; consequently, there are eight $Y_Z^\bullet$ sites in each unit cell. The experimental spectra were well reproduced by spectral simulation (depicted by red lines in the figures), in which the calculated spectra were obtained by superimposing the spectra of eight magnetically inequivalent $Y_Z^\bullet$. The colored curves in Figure 5b show the angular dependence of the effective *g* values.

dx.doi.org/10.1021/ja2000566 |*J. Am. Chem. Soc.* 2011, 133, 4655–4660

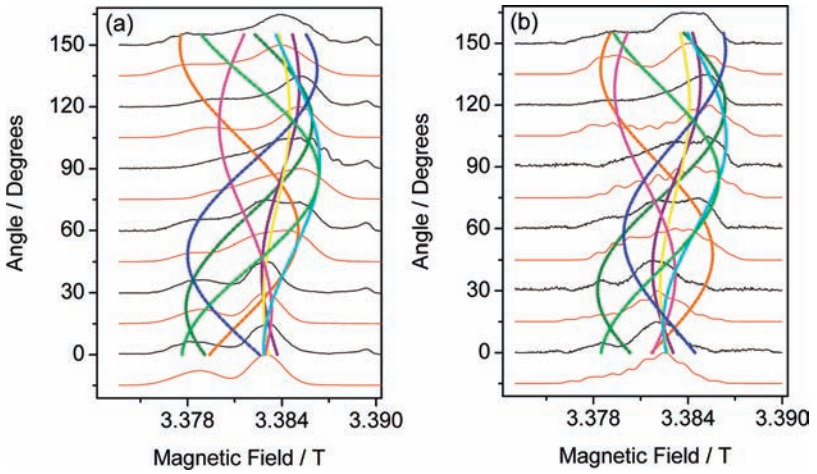

Figure 5. (a) Orientation-dependent W-band EPR spectra of the $Y_D^{\bullet}$ radical in single crystals of PSII from *T. vulcanus*, shown at 30° intervals. Spectra were obtained at 15° intervals at 80 K as the crystal was rotated approximately about the crystallographic *b* axis. (b) Light minus dark-annealed difference spectra corresponding to the EPR of $Y_Z^{\bullet}$. The spectra were recorded in the same orientation as for (a). The black and red lines represent the experimental spectra and the best-fit simulation, respectively. Dotted and colored curves show the angular dependence of the effective *g* values, calculated for the eight symmetric sites within the unit cell.

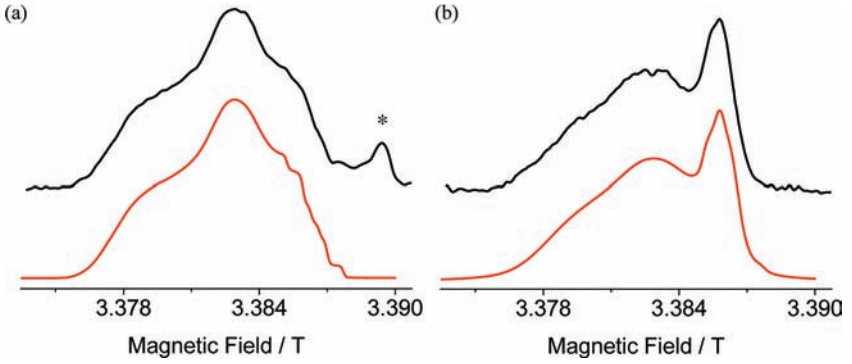

Figure 6. W-band EPR spectra of (a) $Y_D^{\bullet}$ and (b)$Y_Z^{\bullet}$ in frozen solution of PSII from *T. vulcanus* at 80 K. The black and red lines represent the experimental spectra and the best-fit simulation, respectively. The asterisk denotes a signal from a quartz capillary tube color center, which was employed as an internal intensity standard to ensure the difference spectra were correct.

Orientation-dependent EPR spectra of $Y_Z^{\bullet}$ were also recorded for a different crystal. The experimental spectra were well reproduced by spectral simulation, as shown in Figure S4b. The principal values obtained for the *g*-tensor are shown in Table 1; these are in good agreement with those determined independently for the frozen solution (Figure 6b).

Discrimination between PCET Processes in Water Oxidation. As mentioned above, the H-atom abstraction mechanism requires the formation of a tyr—imidazole complex. However, even for the shortest hydrogen-bond length of 1.5 Å (Figure 4a), the calculated g_x-value (~2.0089) of the tyr—imidazole complex was significantly higher than the experimental value (2.00705). It has been demonstrated previously that a lower g_x component for a tyrosine radical is due to the existence of an electropositive environment near the radical, such as an imidazolium cation.[4,30,31] Thus, it was concluded on the basis of W-band EPR spectroscopy that a tyr—imidazolium ion complex is formed in Mn-depleted PSII after photooxidation of the redox-active tyrosine Y_Z, indicating that the imidazole group of D1-His190 is not deprotonated after accepting a proton from Y_Z. This implies that the H-atom abstraction mechanism is incorrect. Extended X-ray absorption fine structure data and crystallographic analysis suggested that Ca^{2+} forms a mixed cluster with four Mn atoms in WOC. Y_Z is ~5 Å from the Ca^{2+} ion and even further from the Mn atoms, with the nearest Mn atom located at ~7 Å. Although these are reasonable distances for electron transfer, they are unreasonable for proton transfer with a short-range character. The structural information supported our results; these are in line with the suggested proton-rocking mechanism,[14−16] which does not require deprotonation from D1-His190. Thus, we can conclude that the proton-transfer process between Y_Z and D1-His190 in Mn-depleted PSII involves a proton-rocking mechanism.

Table 1. Principal Values of the *g*-Tensor of $Y_D^{\bullet}$ and $Y_Z^{\bullet}$, Determined by Analysis of the W-Band Spectra of PSII as Single Crystals and in Frozen Solution

	Y_D			Y_Z		
	g_X	g_Y	g_Z	g_X	g_Y	g_Z
crystal	2.00750	2.00432	2.00219	2.00705	2.00436	2.00219
solution	2.00750	2.00430	2.00219	2.00714	2.00439	2.00219

dx.doi.org/10.1021/ja2000566 |*J. Am. Chem. Soc.* 2011, 133, 4655–4660

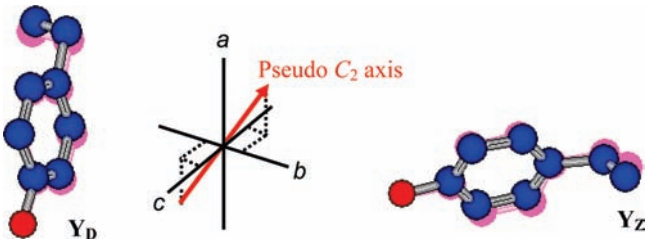

Figure 7. Relative orientations of $Y_D^\bullet$, $Y_Z^\bullet$, and the pseudo-C_2 axis with respect to the crystallographic axes, determined from the W-band EPR. Carbon and oxygen atoms are shown as blue and red circles, respectively. For simplicity, hydrogen atoms are not shown. The pseudo-C_2 axis is inclined relative to the C_2 dimer axis by 7.5°. For the purpose of comparison, the $Y_D^\bullet$ and $Y_Z^\bullet$ orientations from the most recent X-ray structure at 1.9 Å resolution[2b] are shown in pink.

Influence of Mn Depletion on the Molecular Orientation of $Y_Z^\bullet$ Relative to the Crystallographic Axes. In the absence of WOC, Y_Z can be trapped as the neutral radical $Y_Z^\bullet$. To examine the molecular orientation of $Y_Z^\bullet$ relative to the crystallographic axes after Mn depletion, the crystal orientations relative to the magnetic field were determined. In this work, the crystal orientations relative to the magnetic field were determined on the basis of analysis of the orientation-dependent EPR spectra of $Y_D^\bullet$. As fitting parameters, we used the principal values and orientation of the *g*-tensor relative to the crystallographic axes together with the crystal orientation relative to the laboratory frame. Echo-detected field-swept EPR spectra of $Y_D^\bullet$ were obtained at 80 K after dark annealing for 30 min at 253 K, with single crystals of Mn-depleted PSII repeatedly rotated by 15°. The experimental spectra are shown at 30° intervals as black lines in Figure 5a; these were well reproduced by spectral simulation, as depicted by red lines. The colored curves in Figure 5a show the angular dependence of the effective *g* values for the eight symmetric sites within the unit cell. These spectral analyses indicated that the rotation axis of the magnetic field was approximately parallel to the crystallographic *b*-axis. The crystallographic *c*- and *a*-axes are approximately parallel to the direction of the magnetic field at 60° and 150° rotation (Figure 5a), respectively. The orientation-dependent spectra of another crystal of $Y_D^\bullet$, for which the rotation axis was approximately parallel to the crystallographic *a*-axis, were also well reproduced by spectral simulation (Figure S4). The determined principal values of the *g*-tensor, shown in Table 1, are in good agreement with those determined independently from the frozen-solution experiment (Figure 6a). The individual PSII core complexes in the dimer are related to each other by a noncrystallographic C_2 symmetry axis (dimer axis); the orientations with respect to the crystallographic axes are given as direction cosines in the Supporting Information.

The molecular orientations of $Y_Z^\bullet$ relative to the crystal axes were determined using the crystal orientations with respect to the magnetic field deduced from the EPR measurements of $Y_D^\bullet$. The EPR-derived molecular orientations of $Y_D^\bullet$ and $Y_Z^\bullet$ with respect to the crystallographic axes are shown in Figure 7. According to the crystallographic analysis, the cofactors of the electron-transfer chain form two branches, organized symmetrically along a pseudo-C_2 axis, whose direction is depicted as a red arrow in the figure. It was demonstrated by spectral analysis that the C_2 dimer axis is inclined relative to the pseudo-C_2 axis by 7.5°. For the purpose of comparison with the most recent X-ray structure at 1.9 Å resolution,[2b] the $Y_D^\bullet$ and $Y_Z^\bullet$ orientations from the crystal structure are shown in pink. Because $Y_Z^\bullet$ is rapidly reduced in the presence of WOC, it is expected that the orientation of the reduced Y_Z molecule may be determined by X-ray crystallographic analysis including WOC. It is interesting to note that the EPR-derived molecular orientations are almost identical to those obtained from the crystal structure, demonstrating that the orientation of the redox-active tyrosine molecule Y_Z is unchanged during photooxidation. It was concluded that the pattern of hydrogen bonding around the molecule is not influenced drastically by the removal of WOC. In the presence of WOC, intermediates of the S-state transitions can be trapped at liquid helium temperatures, at which $Y_Z^\bullet$ interacts magnetically with WOC.[30−33] Further experiments involving intermediates in the presence of WOC are underway, with the aim of achieving a more detailed understanding of the mechanism of oxygen evolution.

CONCLUSIONS

The *g*-anisotropy of $Y_Z^\bullet$ was highly resolved by W-band EPR spectroscopy using PSII single crystals to discriminate between two different proposed PCET mechanisms. On the basis of the DFT theoretical calculations, the *g* values obtained were consistent with the existence of a tyr−imidazolium ion complex upon one-electron oxidation of Y_Z, indicating that the proton remains on D1-His190 in Mn-depleted PSII. Our experimental data support the proton-rocking mechanism, in which the proton of D1-His190 is transferred back to Y_Z upon rereduction. We determined for the first time the *g*-tensor directions for the redox-active tyrosine radical $Y_Z^\bullet$ relative to the crystal axes. Precise determination of molecular orientation in single crystals of Mn-depleted PSII demonstrated that the molecular orientation of $Y_Z^\bullet$ was unchanged by the removal of WOC.

ASSOCIATED CONTENT

Supporting Information. Effect of NH_2OH concentration on W-band EPR spectra; W-band EPR of radicals in a secondary electron-transfer pathway; DFT optimized structures; single-crystal EPR spectra observed with different crystal orientation from that shown in Figure 5; principal orientations of *g*-tensors; refined hyperfine coupling constants; basis set and density functional dependence of the g_X-component; and Supporting Information references. This material is available free of charge via the Internet at http://pubs.acs.org.

AUTHOR INFORMATION

Corresponding Author
hmatsu@tagen.tohoku.ac.jp

ACKNOWLEDGMENT

This work was partially supported by a Grant-in-Aid for Scientific Research on Priority Areas, "High Field Spin Science in 100T" (No. 451), by the Management Expenses Grants for National Universities Corporations, and by a Grant-in-Aid for Young Scientists (B) from the Ministry of Education, Culture, Sports, Science, and Technology (MEXT), Japan.

REFERENCES

(1) (a) Zouni, A.; Witt, H. T.; Kern, J.; Fromme, P.; Krauss, N.; Saenger, W.; Orth, P. *Nature* **2001**, *409*, 739–743. (b) Guskov, A.; Kern, J.; Gabdulkhakov, A.; Broser, M.; Zouni, A.; Saenger, W. *Nat. Struct. Mol. Biol.* **2009**, *16*, 334–42.

(2) (a) Kamiya, N.; Shen, J. R. *Proc. Natl. Acad. Sci. U.S.A.* **2003**, *100*, 98–103. (b) Umena, Y.; Kawakami, K.; Shen J.-R.; Kamiya, N. *Nature*, in press.

(3) Ferreira, K. N.; Iverson, T. M.; Maghlaoui, K.; Barber, J.; Iwata, S. *Science* **2004**, *303*, 1831–1838.

(4) Faller, P.; Goussias, C.; Rutherford, A. W.; Un, S. *Proc. Natl. Acad. Sci. U.S.A.* **2003**, *100*, 8732–8735.

(5) Hofbauer, W.; Zouni, A.; Bittl, R.; Kern, J.; Orth, P.; Lendzian, F.; Fromme, P.; Witt, H. T.; Lubitz, W. *Proc. Natl. Acad. Sci. U.S.A.* **2001**, *98*, 6623–6628.

(6) Teutloff, C.; Pudollek, S.; Kessen, S.; Broser, M.; Zouni, A.; Bittl, R. *Phys. Chem. Chem. Phys.* **2009**, *11*, 6715–6726 and references therein.

(7) Matsuoka, H.; Furukawa, K.; Kato, T.; Mino, H.; Shen, J.-R.; Kawamori, A. *J. Phys. Chem. B* **2006**, *110*, 13242–13247.

(8) Renger, G.; Renger, T. *Photosynth. Res.* **2008**, *98*, 53–80. McEvoy, J. P.; Brudvig, G. W. *Chem. Rev.* **2006**, *106*, 4455–4483.

(9) Meyer, T. J.; Huynh, M. H. V.; Thorp, H. *Angew. Chem., Int. Ed.* **2007**, *46*, 5284–5304.

(10) McEvoy, J. P.; Brudvig, G. W. *Chem. Rev.* **2006**, *106*, 4455–4483.

(11) Tommos, C.; Tang, X.-S.; Warncke, K.; Hoganson, C. W.; Styring, S.; McCracken, J.; Diner, B. A.; Babcock, G. T. *J. Am. Chem. Soc.* **1995**, *117*, 10325–10335.

(12) Hays, A.-M. A.; Vassiliev, I. R.; Golbeck, J. H.; Debus, R. J. *Biochemistry* **1998**, *37*, 11352–11365.

(13) (a) Hoganson, C. W.; Lydakis-Simantiris, N.; Tang, X.-S.; Tommos, C.; Warncke, K.; Babcock, G. T.; Diner, B. A.; McCracken, J.; Styring, S. *Photosynth. Res.* **1995**, *46*, 177. (b) Hoganson, C. W.; Babcock, G. T. *Science* **1997**, *277*, 1953–1956.

(14) (a) Eckert, H. J.; Renger, G. *FEBS Lett.* **1988**, *236*, 425–431. (b) Renger, G.; Renger, T. *Photosynth. Res.* **2008**, *98*, 53–80.

(15) Hays, A. M. A.; Vassiliev, I. R.; Golbeck, J. H.; Debus, R. J. *Biochemistry* **1999**, *38*, 11852–11865.

(16) Dordrecht, J. W.; Haumann, M.; Ahlbrink, R. M. A.; Clausen, J. *Philos. Trans. R. Soc. London, Ser. B* **2002**, *357*, 1407–1418.

(17) Shen, J. R.; Kamiya, N. *Biochemistry* **2000**, *39*, 14739–14744.

(18) Gromov, I.; Krymov, V.; Manikandan, P.; Arieli, D.; Goldfarb, D. *J. Magn. Reson.* **1999**, *139*, 8–17.

(19) Schwartz, D. A.; Walter, E. D.; McIlwain, S. J.; Krymov, V. N.; Singel, D. J. *Appl. Magn. Reson.* **1999**, *16*, 223–236.

(20) Mino, H.; Astashkin, A. V.; Kawamori, A. *Spectochim. Acta, Part A* **1997**, *53*, 1465–1483.

(21) Matsuoka, H.; Furukawa, K.; Sato, K.; Shiomi, D.; Kojima, Y.; Hirotsu, K.; Furuno, N.; Kato, T.; Takui, T. *J. Phys. Chem. A* **2003**, *107*, 11539–11552.

(22) Iwasaki, M. *J. Magn. Reson.* **1974**, *16*, 417–423.

(23) Klamt, A.; Schüürmann, G. *J. Chem. Soc., Perkin Trans.* **1993**, *2*, 793–805.

(24) Neese, F. *J. Chem. Phys.* **2001**, *115*, 11080–11096.

(25) Hasegawa, K.; Noguchi, T. *Biochemistry* **2005**, *44*, 8865–8872.

(26) Benisvy, L.; Bittl, R.; Bothe, E.; Garner, C. D.; McMaster, J.; Ross, S.; Teutloff, C.; Neese, F. *Angew. Chem., Int. Ed.* **2005**, *44*, 5314–5317.

(27) Stoll, S.; Gunn, A.; Brynda, M.; Sughrue, W.; Kohler, A. C.; Ozarowski, A.; Fisher, A. J.; Lagarias, J. C.; Britt, R. D. *J. Am. Chem. Soc.* **2009**, *131*, 1986–1995.

(28) Fasanella, E.; Gordy, W. *Proc. Natl. Acad. Sci. U.S.A.* **1969**, *62*, 299–304.

(29) Brynda, M.; Britt, R. D. *Res. Chem. Intermed.* **2007**, *33*, 863–883.

(30) Ioannidis, N.; Nugent, J. H. A.; Petrouleas, V. *Biochemistry* **2002**, *41*, 9589–9600.

(31) Koulougliotis, D.; Shen, J. R.; Ioannidis, N.; Petrouleas, V. *Biochemistry* **2003**, *42*, 3045–3053.

(32) Zhang, C.; Styring, S. *Biochemistry* **2003**, *42*, 8066–8076.

(33) Petrouleas, V.; Koulougliotis, D.; Ioannidis, N. *Biochemistry* **2005**, *44*, 6723–6728.